The Astrophysical Journal, 766:78 (15pp), 2013 April 1 doi:10.1088/0004-637X/766/2/78

GALA: AN AUTOMATIC TOOL FOR THE ABUNDANCE ANALYSIS OF STELLAR SPECTRA*

Alessio Mucciarelli[1], Elena Pancino[2,3], Loredana Lovisi[1], Francesco R. Ferraro[1], and Emilio Lapenna[1]
[1] Dipartimento di Fisica & Astronomia, Università degli Studi di Bologna, Viale Berti Pichat 6/2, I-40127 Bologna, Italy; alessio.mucciarelli2@unibo.it, loredana.lovisi@unibo.it, francesco.ferraro3@unibo.it, emilio.lapenna2@unibo.it
[2] INAF-Osservatorio Astronomico di Bologna, Via Ranzani 1, I-40127 Bologna, Italy; elena.pancino@oabo.inaf.it
[3] ASI Science Data Center, I-00044 Frascati, Italy
Received 2012 December 13; accepted 2013 February 12; published 2013 March 11

ABSTRACT

GALA is a freely distributed Fortran code for automatically deriving the atmospheric parameters (temperature, gravity, microturbulent velocity, and overall metallicity) and abundances for individual species of stellar spectra using the classical method based on the equivalent widths of metallic lines. The abundances of individual spectral lines are derived by using the WIDTH9 code developed by R. L. Kurucz. GALA is designed to obtain the best model atmosphere by optimizing temperature, surface gravity, microturbulent velocity, and metallicity after rejecting the discrepant lines. Finally, it computes accurate internal errors for each atmospheric parameter and abundance. GALA is suitable for analyzing both early- and late-type stars, under the assumption of local thermodynamical equilibrium. The code permits us to obtain chemical abundances and atmospheric parameters for large stellar samples in a very short time, thus making GALA a useful tool in the epoch of multi-object spectrographs and large surveys. An extensive set of tests with both synthetic and observed spectra is performed and discussed to explore the capabilities and robustness of the code.

Key words: methods: data analysis – stars: abundances – techniques: spectroscopic

1. INTRODUCTION

The past decade has seen a significant improvement in the study of the chemical composition of stellar populations (in our Galaxy and its satellites) thanks to 8–10 m class telescopes coupled with the design of several multi-object mid-/high-resolution spectrographs, e.g., FLAMES mounted at the Very Large Telescope, AAOmega at the Anglo-Australian Telescope, DEIMOS at the Keck Observatory, and HYDRA at the Blanco Telescope of the Cerro Tololo Inter-American Observatory. These instruments have enabled us to enlarge the statistical significance of the acquired stellar spectra, but they have also required a relevant effort to manage such large databases.

The next advent of new surveys aimed at collecting huge samples of mid- to high-resolution stellar spectra such as, for instance, the European Space Agency *Gaia* mission, the *Gaia*-ESO Survey at the European Southern Observatory (Gilmore et al. 2012), the APOGEE Survey at Apache Point Observatory (Allende Prieto et al. 2008), and the RAVE Survey at the Anglo-Australian Observatory (Steinmetz et al. 2006), will make an enormous volume of data available to the astronomical community in real time. Other spectroscopic surveys have already been performed (e.g., BRAVA (Kunder et al. 2012) and ARGOS (Freeman et al. 2013), both of which are dedicated to the study of the Galactic bulge). Also, other multi-object spectrographs have been planned or proposed over the next several years, i.e., HERMES (Barden et al. 2010) at the Anglo-Australian Observatory, 4MOST (de Jong 2011) at the New Technology Telescope, and MOONS (Cirasuolo et al. 2011) at the Very Large Telescope. This perspective, coupled with the huge amount of high-quality spectra available in the main online archives (which has not yet been fully analyzed), highlights the urgency for developing automatic tools able to rapidly and reliably manage such samples of spectra.

Over the last few decades, several codes aimed at calculating automatic measurements of chemical abundances have been developed. They are mainly based on the comparison between the observed spectrum and grids of synthetic spectra, for instance ABBO (Bonifacio & Caffau 2003), MATISSE (Recio-Blanco et al. 2006), SME (Valenti & Piskunov 1996), SPADES (Posbic et al. 2012), and MyGIsFOS (Sbordone et al. 2010). In particular, in these codes the main effort has been devoted to robustly determining the atmospheric parameters (and hence the elemental abundances) for low (<50) signal-to-noise ratio (S/N) spectra and generally to developing an algorithm able to accurately treat different kinds of stars (in terms of metallicity and stellar parameters).

In this paper, we present and discuss a new code (called GALA) specifically designed for automatically determining atmospheric parameters by using the observed equivalent widths (EWs) of metallic lines in stellar spectra, at variance with the majority of the available automated codes. GALA is a tool developed within Cosmic-Lab, a five-year project funded by the European Research Council and is freely available at the project Web site, http://www.cosmic-lab.eu/Cosmic-Lab/Products.html.

This paper is structured as follows. Section 2 discusses the outline of the classical method to derive the main parameters and the interplay occurring among them, Section 3 describes the algorithm, Section 4 describes the identification and the rejection of the outliers, and Section 5 discusses other aspects of the code. Section 6 provides a complete description of the uncertainties in the calculations. Finally, Sections 7, 8, and 9 discuss a number of tests performed to check the stability and the performances of GALA.

2. THE METHOD

The main advantage of inferring the stellar atmospheric parameters from the EWs is reproducibility: any researcher can

* Based on observations collected at the ESO-VLT under programs 65.L-0165, 165.L-0263, 073.D-0211, 080.D-0368, 083.D-0208, and 266.D-5655 and on data available in the ELODIE archive. This research has also made use of the SIMBAD database, operated at CDS, Strasbourg, France.

directly compare his or her own results for a given star with other analyses based on the same approach. This allows researchers to distinguish between discrepancies due to the method (i.e., the measured EWs) and those due to the physical assumptions of the analysis (model atmospheres, atomic data, etc.). On the other hand, one of the most critical aspects of this method is the particular accuracy needed in the definition of the line list due to excluding blended lines. In fact, the codes developed to calculate the abundance from the measured EWs compare the latter with the theoretical strength of the line, changing the abundance until the observed and theoretical EWs match within a convergence range. The theoretical line profile is usually calculated including the continuum opacity sources but neglecting the contribution of the neighboring lines (see Castelli 2005b for details), hence the spectral lines to be analyzed with this technique are to be checked accurately against blending (a practice not always performed). Aside from this, the use of synthetic spectra also allows us to use blended features (and, in principle, to exploit the information derived from all the pixels), but it is more expensive in terms of computing time because large grids of spectra must be computed at different parameters and with different chemical compositions and each change in the atomic data leads to a recomputation of the synthetic spectra.

2.1. The Classical Spectroscopic Method

The main parameters that define the model atmosphere, namely the effective temperature ($T_{\rm eff}$), the surface gravity ($\log g$), the microturbulent velocity (v_t), and the overall metallicity ([M/H][4]), are constrained by the following.

1. *Temperature.* The best value of $T_{\rm eff}$ is derived by imposing the so-called excitation equilibrium, requiring that there is no correlation between the abundance and the excitation potential χ of the neutral iron lines. The number of electrons populating each energy level is basically a function of $T_{\rm eff}$ according to the Boltzmann equation. If we assume a wrong $T_{\rm eff}$ in the analysis of a given stellar spectrum, we need different abundances for matching the observed profile of transitions with different values of χ. For instance, the use of a value of $T_{\rm eff}$ that is too large will lead to underpopulating the lower energy levels, thus the predicted line profile for low χ transitions will be too shallow and a higher abundance will be needed to match the line profile. On the other hand, a wrong (too low) $T_{\rm eff}$ will lead to a deeper line profile for the low χ transitions. For this reason, a wrong, too large value of $T_{\rm eff}$ will introduce an anticorrelation between abundances and χ, and in the same way, a positive correlation is expected in the case of the adoption of a value of $T_{\rm eff}$ that is too small.
2. *Surface gravity.* The best value of $\log g$ is derived with the so-called ionization equilibrium method, requiring that for a given species, the same abundance (within the uncertainties) has been obtained from lines of two ionization states (typically, neutral and singly ionized lines). Because gravity is a direct measure of the pressure of the photosphere, variations of $\log g$ lead to variations in the ionized lines (which are very sensitive to electronic pressure), while the neutral lines are basically insensitive to this parameter. This method implicitly assumes that the energy levels of a given species are populated according to the Boltzmann and Saha equations (thus, under local thermodynamical equilibrium (LTE) conditions). Possible departures from this assumption (which is especially critical for metal-poor and/or low-gravity stars) could alter the derived gravity when it is derived from the ionization balance because non-LTE effects affect mainly the neutral lines (even if the precise magnitude of the departures from LTE for the iron lines is still a matter of debate). As a sanity check, following the suggestion by Edvardsson (1988, p. 1), surface gravities determined from the ionization equilibria have to be "checked—when possible—with gravities determined from the wings of pressure-broadened metal lines".
3. *Microturbulent velocity.* v_t is computed by requiring that there is no correlation between the iron abundance and the line strength (see Mucciarelli 2011 for a discussion about different approaches). The microturbulent velocity affects mainly the moderate/strong lines located along the flat regime of the curve of growth, while the lines along the linear part of the curve of growth are mainly sensitive to the abundance instead of the velocity fields. The necessity to introduce the microturbulent velocity as an additional broadening (added in quadrature to the Doppler broadening) arises from the fact that the non-thermal motions (basically due to the onset of the convection in the photosphere) are generally not well described by one-dimensional, static model atmospheres. Citing Kurucz (2005, p. 16), "microturbulent velocity is a parameter that is generally not considered physically except in the Sun" because in the Sun, velocity fields can be derived as a function of optical depth through analysis of the intensity spectrum (as performed by Fontenla et al. 1993). For other stars, v_t represents only a corrective factor that minimizes the line-to-line scatter for a given species and compensates (at least partially) for the incomplete description of the convection as implemented in one-dimensional model atmospheres.
4. *Metallicity.* [M/H] is chosen according to the average iron content of a star, assuming [Fe/H] as a proxy for the overall metallicity. Generally, [Fe/H] is adopted as a good proxy of the metallicity because of its large number of available lines, but it does not necessarily indicate the overall metallicity of the studied star. In fact, iron is generally not the most abundant element in stars; elements such as C, N, and O would be the best tracers of stellar metallicity but they are difficult to measure.

Because of its statistical nature, the spectroscopic optimization of all the parameters can simultaneously be performed only if we have a sufficient number of Fe lines, distributed in a large range of EW and χ and in two levels of ionization. Alternatively, $T_{\rm eff}$ and $\log g$ can be inferred from the photometry (for instance with the isochrone-fitting technique or employing empirical or theoretical $T_{\rm eff}$–color relations) or by fitting the wings of damped lines (such as hydrogen Balmer lines or the Mg b triplet) sensitive to the parameters, and only v_t needs to be tuned spectroscopically (following the approach described above). Note that some authors consider the method of deriving the parameters based on these constraints only as sanity checks performed a posteriori on the photometric parameters while other authors rely on these constraints to infer the best parameters.

2.2. The Interplay among the Parameters

In light of the method described above, it is worth bearing in mind that the atmospheric parameters are correlated with each

[4] We adopted the classical bracket notation $[X/H] = A(X)_{\rm star} - A(X)_{\odot}$, where $A(X) = \log N_A/N_H + 12$.

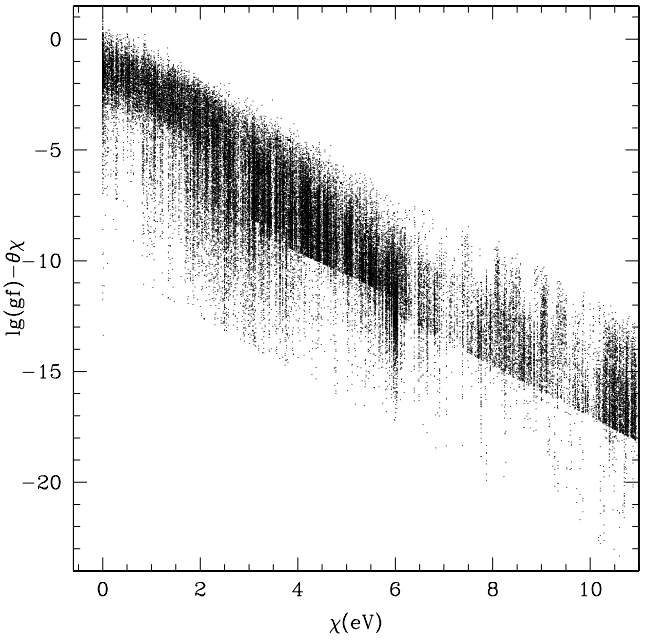

Figure 1. Behavior of the line strength (computed assuming $T_{\rm eff} = 4500$ K) as a function of the excitation potential χ for all the transitions available in the Kurucz/Castelli line list in the range of wavelength $\lambda = 4000$–8000 Å and with $\chi < 10$ eV.

other. In fact, the strongest lines are typically those with low χ: Figure 1 plots all the transitions in the range $\lambda = 4000$–8000 Å and with $\chi < 10$ eV in the Kurucz/Castelli database[5] in the plane χ versus $\log(gf) - \theta\chi$.[6] As mentioned in Section 2.1, $T_{\rm eff}$ and χ are strictly linked and there is also a connection between v_t and the line strength. Hence, the statistical correlation between χ and the line strength leads to a correlation between $T_{\rm eff}$ and v_t. Thus, a variation of $T_{\rm eff}$ implies a variation of v_t. Also, variations of $T_{\rm eff}$ and v_t will change the abundances derived from different levels of ionization (hence, the gravity) in different ways.

Let us consider an ATLAS9 model atmosphere computed with $T_{\rm eff} = 4500$ K, $\log g = 1.5$, $v_t = 2$ km s^{-1}, and [M/H] $= -1.0$ dex (Castelli & Kurucz 2004) and a set of neutral and singly ionized iron lines (predicted to be unblended through the inspection of a spectrum calculated with the same parameters at a spectral resolution of 45,000). The EWs of these transitions are computed by integrating the theoretical line profile through the WID subroutine implemented in the WIDTH9 code (Castelli 2005b). This means that each of these EWs will provide exactly [El/H] $= -1.0$ dex when they are analyzed using the model atmosphere described above.

The analysis of these lines (always adopting the same set of EWs) is repeated investigating a regular grid of the atmospheric parameters, namely $T_{\rm eff} = 3600$–5400 K, $\log g = 0.5$–2.5, $v_{\rm t} = 1.0$–3.0 km s^{-1}, steps of $\delta T_{\rm eff} = 200$ K, $\delta \log g = 0.2$, $\delta v_{\rm t} = 0.5$ km s^{-1}, and assuming for all the models [M/H] $= -1.0$ dex. Figures 2, 3, and 4 display the quite complex interplay occurring among the atmospheric parameters.

1. Figure 2 shows the behavior of the slope S_χ of the A(Fe)–χ relation for the above sample of lines as a function of $T_{\rm eff}$, keeping gravity fixed, but varying the microturbulent velocity. The thick gray line connects points calculated with the original v_t of the model. The global trend is basically linear, at least if we consider a range of ± 1000 K around the original $T_{\rm eff}$. The inset panel shows the behavior of $T_{\rm eff}$ for which S_χ is zero (thus, the best $T_{\rm eff}$) as a function of v_t and considering different gravities. The derived best

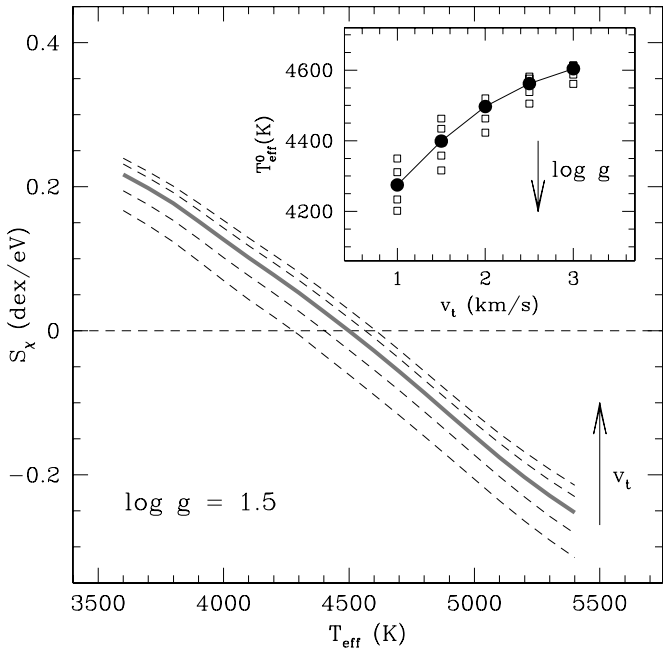

Figure 2. Main panel: behavior of the slope S_χ of the A(Fe)–χ relation as a function of $T_{\rm eff}$ assuming $\log g = 1.5$ and for different values of $v_{\rm t}$ (dashed curves). The thick gray curve represents the behavior computed for the original microturbulent velocity ($v_{\rm t} = 2.0$ km s^{-1}). The horizontal dashed line is the zero value (according to the excitation equilibrium). The inset panel shows the behavior of the best value of $T_{\rm eff}$ (for which $S_\chi = 0$) as a function of the v_t used (empty squares) and for different gravities; black points refer to the original gravity ($\log g = 1.5$).

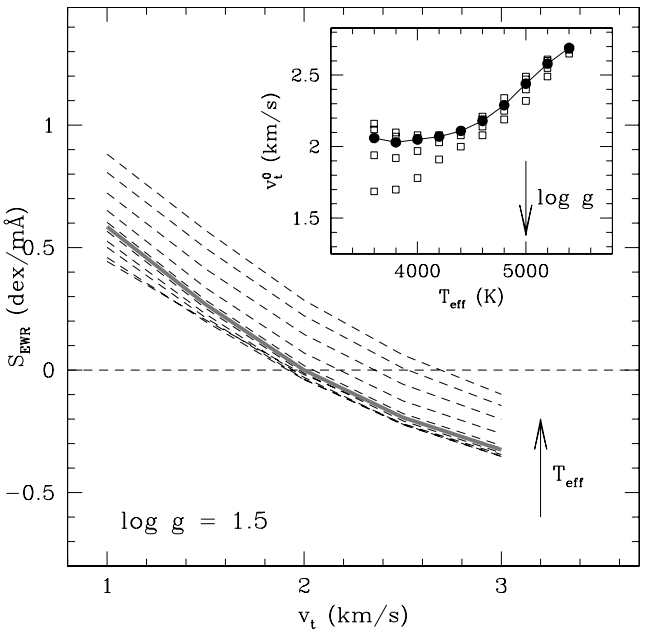

Figure 3. Main panel: behavior of the slope $S_{\rm EWR}$ of the A(Fe)–EWR relation as a function of $v_{\rm t}$ assuming $\log g = 1.5$ and for different values of $T_{\rm eff}$ (dashed curves). The thick gray curve represents the behavior computed for the original temperature ($T_{\rm eff} = 4500$ K). The horizontal dashed line is the zero value. The inset panel shows the behavior of the best value of the microturbulent velocity $v_{\rm t}$ (for which $S_{\rm EWR} = 0$) as a function of the $T_{\rm eff}$ used (empty squares) and for different values of gravities; black points refer to the original gravity ($\log g = 1.5$).

[5] http://wwwuser.oat.ts.astro.it/castelli/linelists.html

[6] The term $\log(gf) - \theta\chi$ is used as a theoretical proxy of the line strength, where $\log(gf)$ is the oscillator strength and $\theta = 5040/T_{\rm eff}$ eV^{-1}.

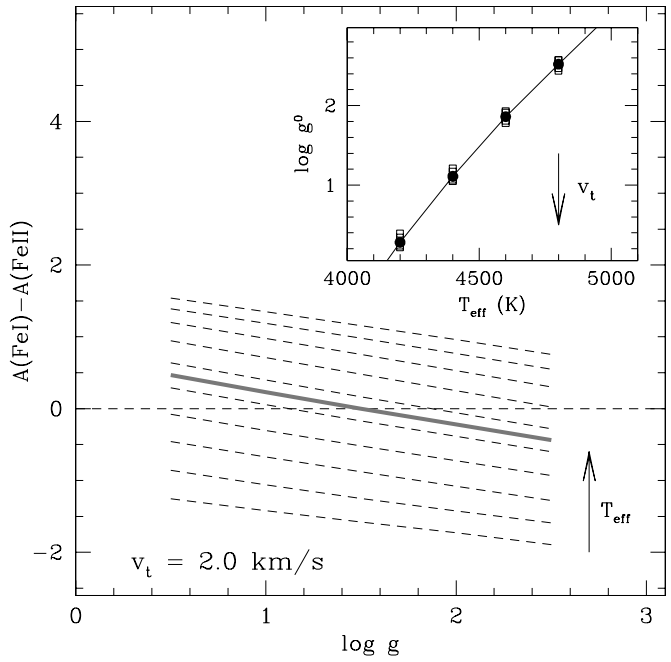

Figure 4. Main panel: behavior of the difference between A(Fe I) and A(Fe II) as a function of log g assuming $v_t = 2.0$ km s^{-1} and for different values of $T_{\rm eff}$ (dashed curves). The thick gray curve represents the behavior computed for the original temperature ($T_{\rm eff} = 4500$ K). The horizontal dashed line is the zero value (according to the ionization equilibrium). The inset panel shows the behavior of the best log g (for which A(Fe I) = (Fe II)) as a function of the $T_{\rm eff}$ used (empty squares) and for different gravities; black points refer to the original microturbulent velocity ($v_t = 2.0$ km s^{-1}).

temperature increases with increasing v_t (at fixed log g); gravity only has a second-order effect and it does not change the general behavior of the best $T_{\rm eff}$ as a function of v_t.

2. Figure 3 summarizes the behavior of the slope $S_{\rm EWR}$ of the A(Fe)–EWR relation as a function of v_t (where EWR indicates the reduced EW, defined as EWR = log(EW/λ)), keeping gravity fixed at the original value but varying $T_{\rm eff}$. For a given temperature, the slope decreases with increasing v_t, with a behavior that becomes less steep at v_t larger than the original value. The effect of the $T_{\rm eff}$ is appreciable for $T_{\rm eff}$ larger than the original value, while for lower $T_{\rm eff}$ all the curves are very similar to each other. The inset shows the change of the best value of v_t (for which the slope of the A(Fe)–EWR relation is zero) as a function of $T_{\rm eff}$ and for different values of log g. The observed trend is quite complex; basically, we note that the best value of v_t is very sensitive to $T_{\rm eff}$ when the latter is overestimated with respect to the true temperature, but with a negligible dependence on gravity, while the behavior is the opposite when $T_{\rm eff}$ is underestimated, with a degeneracy between $T_{\rm eff}$ and the best $v_{\rm t}$ but a consistent dependence on gravity.

3. Figure 4 shows the behavior of the difference between A(Fe I) and A(Fe II) as a function of log g, assuming $v_t = 2$ km s^{-1} and for different values of $T_{\rm eff}$. The general behavior is linear and the iron difference increases considerably with increasing temperature. The best value of gravity (see the inset in Figure 4) is highly sensitive to changes in $T_{\rm eff}$, with $\delta\log g/\delta T_{\rm eff} \simeq 1$ dex/300 K in the investigated case, but for a fixed $T_{\rm eff}$ turns out to be marginally sensitive to v_t (this is due to the fact that the Fe II lines are basically distributed in strength in a similar way to the Fe I lines).

It is important to bear in mind that these considerations are appropriate for the investigated case of a late-type star but the dependencies among the parameters can be different for different regimes of atmospheric parameters and/or metallicity. However, the example presented above demonstrates that an analytic approach to deriving the best model atmosphere is discouraged because it requires precise topography of the parameter space and inspection of a large number of model atmospheres.

3. GALA

GALA is a program written in standard Fortran 77 that uses the WIDTH9 code developed by R. L. Kurucz in its Linux version (Sbordone et al. 2004) to derive the chemical abundances of single, unblended absorption lines starting with their measured EWs. We used our own version of WIDTH9, modified in order to have a more flexible format for the input/output files with respect to the standard version of the code available on F. Castelli's Web site, while the input physics and the method for deriving the abundances are unchanged.

GALA is specifically designed to

1. choose the best model atmosphere by using the observed EWs of metallic lines,
2. manage the input/output files of the WIDTH9 code, and
3. provide statistical and graphical tools to evaluate the quality of the final solution and the uncertainty of the derived parameters.

GALA is designed to handle both ATLAS9 (Castelli & Kurucz 2004) and MARCS (Gustafsson et al. 2008) model atmospheres which are the most popular employed data sets for models. The current version has been compiled with the Intel Fortran Compiler (versions 11, 12, and 13) and tested on the Leopard, Snow Leopard, and Lion Mac OSX systems, and on the Ubuntu, Fedora, and Mandriva Linux platforms.

3.1. Optimization Parameters

GALA has been designed to perform classical chemical analysis based on the EWs in an automated way. The user can choose to perform a full spectroscopic optimization of the parameters or to optimize only some parameters, keeping the other parameters fixed to the specified input values.

The algorithm optimizes one parameter at a time, checking continuously if the new value of a given parameter changes the validity of the previously optimized ones.

For each atmospheric parameter X (corresponding to $T_{\rm eff}$, log g, v_t, and [M/H]) we adopt a specific optimization parameter $C(X)$, defined such that it turns out to be zero when the best value of the X parameter has been found. Hence, GALA varies X until a positive/negative pair of the $C(X)$ is found, thus bracketing the zero value corresponding to the best value. Thus, the condition $C(\tilde{X}) = 0$ identifies $X = \tilde{X}$ as the best value of the given parameter. Finally, the best solution converges to a set of parameters that simultaneously verifies the constraints described in Section 2.1. When the atmospheric parameters have been found, the abundances of all the elements for which EWs have been provided are derived.

According to the literature, the adopted values of $C(X)$ have been defined to parameterize the conditions listed in Section 2.1, namely, the following.

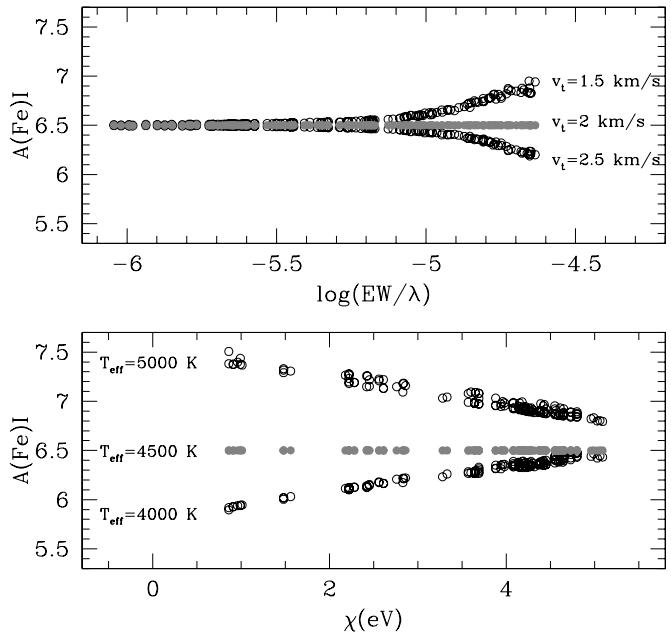

Figure 5. Upper panel: behavior of A(Fe I) as a function of the reduced equivalent widths for a set of theoretical EWs obtained from a model atmosphere computed with $T_{\rm eff} = 4500$ K, log $g = 2.0$, and $v_t = 2$ km s^{-1}. The derived abundances are obtained by adopting the correct value of v_t (gray points) and two *wrong* values of v_t (open circles). Lower panel: behavior of A(Fe I) as a function of the excitation potential for the same set of theoretical EWs. Gray points are the results obtained by analyzing the lines with the correct value of $T_{\rm eff}$, while the empty circles are obtained by overestimating/underestimating $T_{\rm eff}$ by ±500 K.

1. The angular coefficient of the A(Fe)–χ relation (S_χ) for constraining $T_{\rm eff}$. The lower panel of Figure 5 shows the change of this slope for a set of theoretical EWs computed with the correct $T_{\rm eff}$ (gray points) and with temperatures varied by ±500 K (empty points). The variation of $T_{\rm eff}$ produces a change in the slope (but also a change in the y-intercept).
2. The angular coefficient of the A(Fe)–EWR relation ($S_{\rm EWR}$) for constraining v_t. The upper panel of Figure 5 shows the same set of theoretical EWs analyzed with different values of v_t.
3. The difference of the mean abundances obtained from Fe I and Fe II lines for constraining the gravity.
4. The average Fe abundance for constraining the metallicity of the model.

If the errors in the EW measurement ($\sigma_{\rm EW}$) are provided as input, the slopes are computed by taking into account the abundance uncertainties of the individual lines; the uncertainty on the iron abundance of a given line is estimated from the difference of the iron abundance computed for the input EW and for EW+$\sigma_{\rm EW}$.[7] In the A(Fe)–χ plane the uncertainties of χ are reasonably assumed to be negligible because the uncertainties of χ are typically less than 0.01 eV, while in the A(Fe)–EWR plane the least-squares fit takes into account the uncertainties in both the axes (following the prescriptions by Press et al. 1992).

The flexibility of GALA permits us to simultaneously deal with stars of different spectral types. This is done by considering that a large number of Fe I lines are generally available for F–G–K spectral type stars, whereas they are less numerous (or lacking) in O–B–A stars, for which a large number of Fe II lines are typically available. Also, in some spectral regions there is a large number of lines for other iron-peak elements (mainly Ni, Cr, and Ti). For this reason, GALA is designed to optimize the parameters using lines other than Fe I by appropriately configuring the code. In the following, we will refer to the optimization made by using Fe I for $T_{\rm eff}$ and v_t, but our considerations are also valid for other elements with a sufficient number of lines.

[7] The uncertainties in A(Fe) are assumed to be symmetric with respect to the variations of EW (±$\sigma_{\rm EW}$); we checked that this assumption is correct at the level of ∼0.01 dex.

3.2. The Main Structure

GALA is structured in three main working blocks.

1. The "guess" working block is aimed at finding the presumed, or guessed, atmospheric parameters in a fast way (this is especially useful in cases of large uncertainties or when one lacks a first-guess value for the parameters).
2. The "analysis" working block finds the best model atmosphere through a local minimization starting with the guessed parameters provided by the user or obtained through the previous block.
3. The "refinement" working block refines the solution, starting with the atmospheric parameters obtained in the previous block.

GALA can be flexibly configured to use different combinations of the three main working blocks. We defer to Section 8.4 the discussion of the effects of the working blocks. In the following, we describe the algorithm of each block and the cases in which each is recommended.

3.2.1. Guess Working Block

If the atmospheric parameters are poorly known, this working block verifies them quickly by exploring the parameter space in a coarse grid. Thus, it saves a large amount of time if the initial parameters are far away from the correct solution.

1. As a first step, the abundances for each line are derived using the input parameters and some lines are labeled as outliers and excluded from the analysis (the criteria of the rejection are described in Section 4). The surviving lines will be used in this working block and no other line rejection will be performed until convergence.
2. The metallicity of the model is eventually readjusted according to the average iron abundance.
3. S_χ is computed with the input $T_{\rm eff}$ and with a $T_{\rm eff}$ varied by +500 K (if S_χ is positive) or −500 K (if S_χ is negative). This procedure is repeated until a pair of positive/negative values of S_χ is found, thus to bracket the $T_{\rm eff}$ value for which $S_\chi = 0$. The behavior of S_χ as a function of $T_{\rm eff}$ is described with a linear relation, finding the value of $T_{\rm eff}$ for which $S_\chi = 0$. The description of this relation with a linear fit is legitimate as long as the employed $T_{\rm eff}$ range is relatively small (in this case 500 K), because for a larger range, the behavior of S_χ as a function of $T_{\rm eff}$ could become nonlinear (mainly due to interplay with the other parameters).
4. The new value of $T_{\rm eff}$ is adopted to find a new value of v_t, following the same approach used for $T_{\rm eff}$ and searching for a positive/negative pair of $S_{\rm EWR}$ over a range of 0.5 km s^{-1}.
5. Finally, a new value of log g is found, starting with the $T_{\rm eff}$ and v_t derived above by searching for a positive/negative pair of Δ(Fe) over a range of 0.5 dex in gravity.

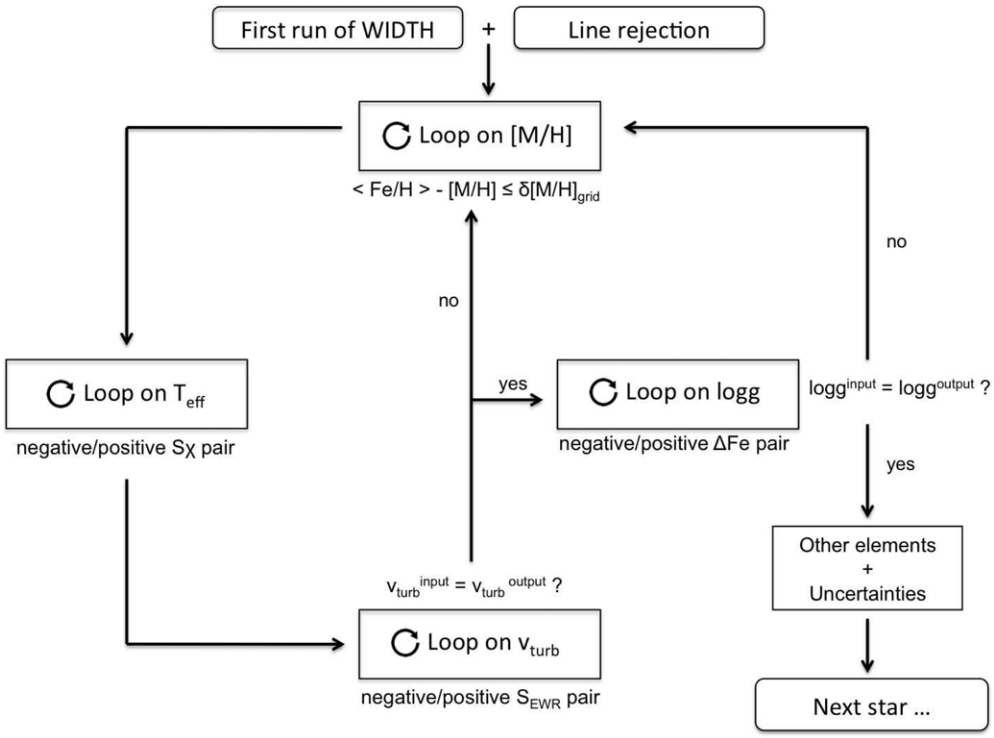

Figure 6. Flow diagram for the analysis working block of GALA (see Section 3.2 for details).

The entire procedure (from the optimization of [M/H] to that of log g) is repeated for a number of iterations chosen by the user and finally a new set of input parameters is found. Generally, three or four iterations are sufficient to find a good solution. The final solution is accurate enough to identify the neighborhood of the real solution in the parameter space but it could be unreliable since it needs to be checked for covariances among the parameters (which is the task of the analysis working block).

3.2.2. Analysis Working Block

This working block performs a complete optimization starting from the input parameters provided by the users or from those obtained with the guess working block. This block is developed to find a robust solution under the assumption that the input values are reasonably close to the real solution. When good priors are available (for instance, in the case of stellar cluster stars) this block is sufficient for finding the solution without the use of the guess block. Otherwise, when the guess model is uncertain (for instance, in the case of field stars for which reddening, distance, and evaluative mass could be highly uncertain, or, generally, in the case of inaccurate photometry), the analysis block is recommended to be used after the guess block. Figure 6 shows a flow chart the main steps of this working block. The following iterative procedure is performed.

1. The procedure starts by computing the abundances using the guessed parameters and performing a new line rejection (independent of that of the previous block). At variance with the previous working block, now the parameters are varied by small steps configured by the user.
2. The model metallicity is refined to match the average iron abundance.
3. A new model with different values of $T_{\rm eff}$ is computed, according to the sign of S_χ of the previous model (i.e., a negative slope indicates an overestimated $T_{\rm eff}$ and vice versa). New models, varying only $T_{\rm eff}$, are computed until a pair of negative/positive S_χ is found. Thus, these two values of $T_{\rm eff}$ identify the range of $T_{\rm eff}$ where the slope is zero. $T_{\rm eff}$ corresponding to the minimum $|S_\chi|$ is adopted.
4. The same procedure is performed for v_t. If the final value of v_t is different from that used in the previous loop, GALA goes back to (2), checking if the new value of v_t needs a change in [M/H] and $T_{\rm eff}$. Otherwise, the procedure moves on to the next loop.
5. The surface gravity is varied until a positive/negative pair of Δ(Fe) is found. If the output log g differs from the input value, GALA returns to (2) with the last obtained model atmosphere and the entire procedure is repeated.
6. When a model that satisfies all four constraints is found, the procedure ends and the next star is analyzed.

We stress that the method employed in this working block is very robust but it has the disadvantage of being slow if the guessed parameters are far from the local solution.

3.2.3. Refinement Working Block

This block allows us to repeat the previous working block using the solution obtained in the previous block as a starting point. A new rejection of the outliers is performed and the same approach as the analysis working block is used. This block can be useful to refine locally the solution when the first block is switched off.

The main advantage of the refinement working block is that the new line rejection is performed using accurate atmospheric parameters (obtained from the analysis working block). As will be discussed in Section 4, the line rejection performed on abundance distributions obtained with wrong parameters can be risky, losing some useful lines.

4. WEEDING OUT THE OUTLIERS

The detection and the rejection of lines with discrepant abundances are crucial aspects of the procedure and require some additional discussion. Before ruling out a line from the line list, we need to understand the origin of the detected discrepancy. Basically, the main reasons for a discrepant abundance are:

1. inaccurate atomic data (i.e., oscillator strengths) that can underestimate or overestimate the abundance,
2. unrecognized blends with other lines (providing systematically overestimated abundances), and
3. inaccurate EW measurement.

The first two cases can be partially avoided by making an effort during the definition of the adopted line list to include only transitions with accurate log (gf) and checking each transition against blending according to the atmospheric parameters and the spectral resolution.

GALA rejects lines according to the following criteria.

1. Lines weaker or stronger than the input EWR thresholds are rejected in order to exclude either weak and/or strong lines. In fact, weak lines can be heavily affected by noise whereas strong lines can be too sensitive to v_t and/or they can have damping wings for which the fit with a Gaussian profile could be inappropriate, providing a systematic underestimate of the EW.
2. Lines whose uncertainty on the EW measurement is larger than an input threshold chosen by the user and expressed as a percentage are rejected. Note that not all the codes developed to measure EWs provide an estimate of the EW error despite the importance of this quantity. For instance, among the publicly available codes aimed at measuring EWs, DAOSPEC (Stetson & Pancino 2008) and EWDET (Ramirez et al. 2001) provide accurate uncertainty evaluations for each line, while SPECTRE (Fitzpatrick & Sneden 1987) and ARES (Sousa et al. 2007) do not include EW error calculations. For this reason, GALA works even if σ_{EW} is not provided, although this affects the final solution accuracy because all the transitions will be weighed equally despite their different measurement qualities.
3. Lines are rejected according to their distance from the best-fit lines computed in the A(Fe)–χ and A(Fe)–EWR planes through a σ rejection algorithm. A σ rejection from the best-fit lines in the planes used for optimization is more robust with respect to a simple σ rejection based on the abundance distribution. In the latter case, there is a risk of losing some lines that important for the analysis, thus biasing the results. Figure 7 explains this aspect: we consider a synthetic spectrum of a giant star ($T_{\rm eff}$ = 4500 K) and measure the EWs after the injection of Poissonian noise in the spectrum in order to reproduce a reasonable good S/N (∼30). Figure 7 shows the distribution of the Fe I lines in the A(Fe)–χ plane when the chemical analysis is performed by using a wrong model atmosphere with $T_{\rm eff}$ = 5200 K (thus leading to an anticorrelation between A(Fe I) and χ). In the upper panel the outliers were rejected according to the median value of the abundance distribution, shown as a gray solid line, while the two dashed lines mark the $\pm 3\sigma$ level and black points are the surviving lines. In the lower panel, the rejection is performed according to the distance from the best-fit line (shown with the solid line while the two dashed lines mark the $\pm 3\sigma$ level). It is evident that in the first case the majority of the discarded lines are those with low χ (thus, the most sensitive to the $T_{\rm eff}$ changes), with the risk of introducing a bias in the $T_{\rm eff}$ determination. On the other hand, the method of rejection shown in the lower panel of Figure 7 preserves the low-χ lines, guaranteeing the correctness of the final solution.

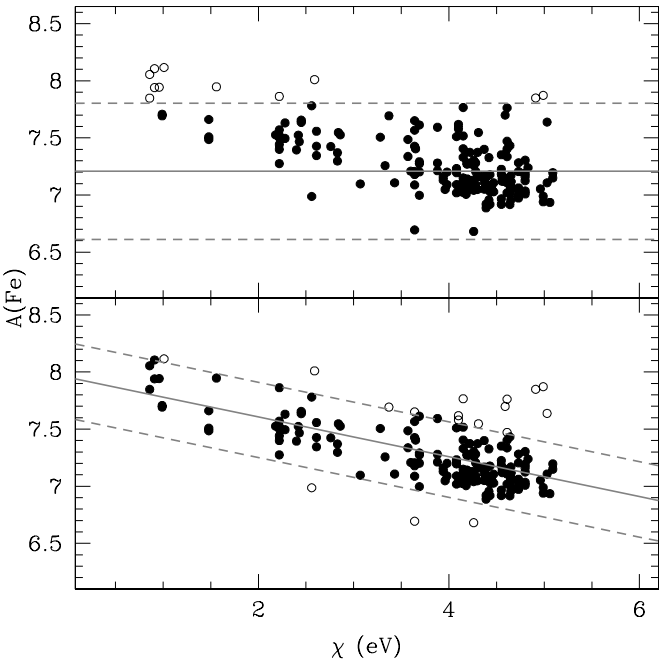

Figure 7. Behavior of the Fe I abundances as a function of the excitation potential for a synthetic spectrum computed assuming $T_{\rm eff}$ = 4500 K but analyzed with a model atmosphere with $T_{\rm eff}$ = 5200 K. Black circles are the lines that survived after the line-rejection procedure and empty points are the rejected lines. The upper panel shows the results of adopting a rejection based on the abundance distribution; the solid line indicates the median abundance and the dashed lines mark the $\pm 3\sigma$ level. The lower panel shows the results using the procedure employed by GALA: the solid line is the best-fit line and the dashed lines mark $\pm 3\sigma$ from the best-fit line.

An important point is that the outlier rejection in GALA is not performed independently in each iteration of the code, but only at the beginning of each working block. This is especially important because it allows us to use always the same sample of lines during the optimization process, avoiding the risk of introducing spurious trends in the behavior of the given optimization parameter as a function of the corresponding atmospheric parameters. In fact, the values of $C(X)$ derived from two different sets of lines of the same spectrum but for which an independent rejection of the outliers has been performed cannot be directly compared to each other to derive X. In particular, this effect is magnified in cases of small numbers of lines where the impact of the rejection of lines can be critical.

5. MORE DETAILS

5.1. A Comment about Gravity

The most difficult parameter to constrain with the classical spectroscopic method is gravity. This is because of the relatively small number of available Fe II lines, which can vary in the visual range from a handful of transitions up to ∼20, depending on the spectral region and/or the metallicity (for instance, some high-resolution spectra with a small wavelength coverage, such as the GIRAFFE at VLT or the Hydra at the BlancoTelescope spectra, can totally lack Fe II lines).

GALA is equipped with different options for optimizing log g.

1. The normal optimization is computed using the difference between the average abundances from neutral and singly ionized iron lines (as described above).
2. The gravity is computed from the Stefan–Boltzmann equation by providing for input the term $\epsilon = \log(4GM\pi\sigma/L)$, where G is the gravitational constant, σ is the Boltzmann constant, and M and L are, respectively, the mass and the luminosity of the star. Thus, during the optimization process, gravity is recomputed (as $\log g = \epsilon - 4\log T_{\rm eff}$) in each iteration according to the new value of $T_{\rm eff}$.
3. Gravity is computed by assuming a quadratic relation $\log g = A + B\,T_{\rm eff} + C\,T_{\rm eff}^2$ and providing as input the coefficients A, B, and C. This option is useful when, for instance, the investigated stars belong to the same stellar cluster and log g and $T_{\rm eff}$ can be parameterized by a simple relation (i.e., such as that described by a theoretical isochrone for a given evolutionary stage).

The user can choose the way to treat log g (fixed or optimized following one of the methods described above); if optimization of log g from the iron lines is requested but no Fe II lines are available, GALA will try to use the second option (lines of other elements in different stages of ionization), or eventually will fix log g to the input value.

5.2. Model Atmospheres

The algorithm used in GALA is basically independent of the code adopted to derive the abundances and of the model atmospheres. GALA is designed to manage the two most used and publicly available model atmospheres, namely, ATLAS9 and MARCS.

1. *ATLAS9.* The suite of Kurucz codes represents the only suite of open-source and free programs to include the different aspects of the chemical analysis (model atmospheres, abundance calculations, spectral synthesis), allowing any user to compute new models and upgrade parts of the codes. GALA includes a dynamic call for the ATLAS9 code.[8] Any time GALA needs to investigate a given set of atmospheric parameters, ATLAS9 is called, a new model atmosphere is computed, and finally, it is stored in a directory. The directory is checked by GALA whenever a model atmosphere is requested and ATLAS9 is called only if the model is lacking. The convergence of the new model atmosphere is checked for each atmospheric layer. Following the prescriptions by Castelli (1988), we require errors less than 1% and 10% for the flux and the flux derivative, respectively. Additional information about the calculation of each model atmosphere is saved. In the current version, GALA is able to manage the grid of ATLAS9 models by Castelli & Kurucz (2004) and the new grid of models calculated by Mészáros et al. (2012) for the APOGEE survey.
2. *MARCS.* At variance with ATLAS9, for the MARCS models, the code to compute new model atmospheres is not released to the community. However, the Uppsala group provides a large grid of the MARCS models on their Web site.[9] When GALA works with these grids (including both plane-parallel and spherical symmetry), new models are computed by interpolating the Uppsala grid using the code developed by T. Masseron (Masseron 2006).[10] This code has been modified in order to put the interpolated MARCS models in ATLAS9 format to use with WIDTH9.

Note that the automatization of the chemical analysis based on EWs needs a wide grid of model atmospheres (both to interpolate and compute new models) linked to the code in order to freely explore the parameter space. Thus, GALA is linked to the ATLAS9 grid both with solar-scaled and α-enhanced chemical composition and to the MARCS grid with standard composition. Also, the use of other models or model grids can be easily implemented in the code. Sometimes, peculiar analyses or tests need to use specific models, for instance for the Sun (see the set of solar model atmospheres available from F. Castelli's Web site) or with arbitrary chemical compositions, such as those computed with the ATLAS12 code (Castelli 2005a). When a specific, single model is called, all the optimization options are automatically switched off.

5.3. Exit Options

GALA is equipped with a number of exit flags in order to avoid infinite loops or unforeseen cases stopping the analysis of the entire input list of stars. Here we summarize the main exit options.

1. The user can set among the input parameters the maximum number of iterations allowed for each star. When the code reaches this value, it stops the analysis, moving to the next star. Generally, this parameter depends on the adopted grid steps and whether or not the input atmospheric parameters are close to the real parameters. When the guess working block is used, the analysis block typically converges in 3–5 iterations.
2. If the dispersion around the mean of the abundances of the lines used for the optimization (after the line rejection) exceeds a threshold value, GALA skips the star. In fact, very large dispersions can possibly suggest some problems in the EW measurements.
3. If the number of lines used for the optimization (after the line rejection) is smaller than a threshold, the optimization is not performed and the atmospheric parameters are fixed to the input guessed values.
4. The procedure is stopped if the requested atmospheric parameter is outside the adopted grid of model atmospheres.
5. GALA skips the analysis of the star if the call to the model atmosphere fails (problems in the ATLAS9 model computation or in the MARCS model interpolation) and the required model is not created. Otherwise, if the ATLAS9 model is calculated but some atmospheric layers do not converge (according to the criteria discussed above), GALA continues the analysis but it advises the user of the number of unconverged layers.

6. UNCERTAINTIES

The code is equipped with different recipes to compute the uncertainties on each derived abundance. Several sources of error can affect the determination of chemical abundances, mainly the uncertainties due to the EW measurements and to the adopted $\log(gf)$ (that are random errors from line to line)

[8] The ATLAS9 source code is available at the Web site http://wwwuser.oat.ts.astro.it/castelli/sources/atlas9codes.html.
[9] http://marcs.astro.uu.se/
[10] The original code is available at http://marcs.astro.uu.se/software.php.

and those arising from the choice of the atmospheric parameters (that are random errors from star to star but systematic from line to line in a given star). These uncertainties are quantified by GALA while other sources of errors (as the choice of the abundance calculation code or the adoption of the grid of model atmospheres) are neglected because of *external* errors considered.

6.1. Statistical Errors in Abundance

The statistical uncertainty on the abundance of each element is computed by considering only the surviving lines after the rejection process (see Section 4). When the uncertainty on the EW is provided for each individual line (thus allowing us to compute the abundance error for each transition), the mean abundance is computed by weighing the abundance of each line on its error, otherwise simple average and dispersion are computed. For those elements for which only one line is available, the error in abundance is obtained by varying the EW of $1\sigma_{\rm EW}$ (if the EW uncertainties are provided). Otherwise, the adopted value is zero. As customary, the final statistical error on the abundance ratios is defined as $\sigma/\sqrt{N_{\rm lines}}$.

6.2. Uncertainties on the Atmospheric Parameters

GALA estimates the internal error for each stellar parameter that has been derived from the spectroscopic analysis. The uncertainties of $T_{\rm eff}$, v_t, and log g are estimated propagating the errors of the corresponding optimization parameter:

$$\sigma_{X_{\rm i}} = \frac{\sigma_{C(X_{\rm i})}}{\left(\frac{\delta C(X_{\rm i})}{\delta X_{\rm i}}\right)},$$

where $X_{\rm i}$ are $T_{\rm eff}$, log g, and v_t; $C(X_{\rm i})$ indicates the optimization parameters defined in Section 3.1; and $\sigma_{C(X_{\rm i})}$ are the corresponding uncertainties.

The terms $\delta C(X_{\rm i})/\delta X_{\rm i}$ (which parameterize how the slopes and the iron difference vary with the appropriate parameters) are calculated numerically by varying $X_{\rm i}$ locally around the final best value, assuming the step used in the optimization process and recomputing the corresponding $C(X_{\rm i})$.

The terms $C(X_{\rm i})$ are computed by applying a jackknife bootstrapping technique (see Lupton 1993). The quoted quantities are recomputed by leaving out one different spectral line from the sample each time (thus, given a sample of N lines, each $C(X)$ is computed N times by considering a subsample of $N-1$ lines). The uncertainty on the parameter X is $\sigma_{\rm Jack} = \sqrt{N-1}\sigma_{\rm sub}$, where $\sigma_{\rm sub}$ is the standard deviation of the $C(X)$ distribution derived from N subsamples. The $\sigma_{\rm Jack}$ takes into account the uncertainty arising from the sample size and the line distribution, and this resampling method is especially useful for estimating the bias arising from the lines' statistics. Note that the computation of the slopes is performed taking into account the effect of the EW and abundance uncertainties of each individual line. Thus, the uncertainty in the atmospheric parameter $X_{\rm i}$ becomes

$$\sigma_{X_{\rm i}} = \frac{\sigma^{\rm Jack}_{C(X_{\rm i})}}{\left(\frac{\delta C(X_{\rm i})}{\delta X_{\rm i}}\right)}.$$

It is worth noting that these uncertainties represent the internal error in the derived parameters and are strongly dependent on the number of used lines and on the distribution of the lines (weak and strong transitions for the estimate of v_t and low- and high-χ lines for $T_{\rm eff}$). Other factors that can affect the determination of the parameters (for instance, the threshold adopted in the EWs and in $\sigma_{\rm EW}$) are not included in the error budgets and they can be considered external errors. Finally, the error due to the adopted grid size could be considered a systematic uncertainty (being the same for all the analyzed stars) and eventually added in quadrature to the internal error estimated by GALA.

6.3. Abundance Uncertainties Due to the Atmospheric Parameters

The evaluation of the uncertainties arising from the atmospheric parameters is a more complex task. Generally, these errors are referred to as "systematic" uncertainties but this nomenclature is rather imprecise. In fact, the variation of a given parameter changes the abundance derived from the lines of the same element in a similar way (for instance, an increase of $T_{\rm eff}$ increases the abundance of all the iron lines). However, this error will be different from star to star due to the different numbers of lines, strength and χ distributions, EW quality, and so on. Thus, the uncertainties from the atmospheric parameters should be considered random errors when we compare different stars (but they are systematic uncertainties from line to line).

Several recipes are proposed in the literature. The most common method is to recompute the abundances, each time changing only one parameter, and keeping the other ones fixed to their best estimates. Then, the corresponding variations in the abundances are added in quadrature. This approach is the most conservative because it neglects the covariance terms arising from the interplay among the parameters (see Section 2.2), providing only an upper limit for the total error budget.

GALA follows the approach described by Cayrel et al. (2004) to naturally take into account the covariance terms. When the optimization process is ended, the analysis is repeated by altering the final $T_{\rm eff}$ by $+\sigma_{T_{\rm eff}}$ and $-\sigma_{T_{\rm eff}}$ (these uncertainties are calculated as described in Section 6.2), and re-optimizing the other parameters. The net variation of each chemical abundance with respect to the original value is assumed as final uncertainty due to the atmospheric parameters and naturally including the covariance terms. Additionally, upon request, the abundance variations are also calculated following the classical approach of varying only one parameter each time (keeping the other parameters fixed), leaving the user free to use this information as preferred.

6.4. Quality Parameter for the Final Solution

GALA also provides a check parameter, useful for judging the quality of the global solution and for rapidly identifying stars with unsatisfactory solutions. For each model used during the optimization process, a merit function $F_{\rm merit}$ is defined as

$$F_{\rm merit} = \sqrt{\left(\frac{S_\chi}{\sigma^{S_\chi}_{\rm Jack}}\right)^2 + \left(\frac{S_{\rm EWR}}{\sigma^{\rm EWR}_{\rm Jack}}\right)^2 + \left(\frac{\Delta{\rm Fe}}{\sigma^{\Delta{\rm Fe}}_{\rm Jack}}\right)^2},$$

taking into account the values of the optimization parameters and the corresponding uncertainties. In an ideal case, $F_{\rm merit}$ is zero if the three optimization parameters are exactly zero. Generally, all the solutions with $F_{\rm merit} \simeq 1$ are valid and equally acceptable, while values of $F_{\rm merit} \gg 1$ are suspect and point out that at least one of the parameters is not well constrained within the quoted uncertainty. Note that $F_{\rm merit}$ provides only an indication of whether or not the solution is acceptable, but it does not specify which parameter is not well defined.

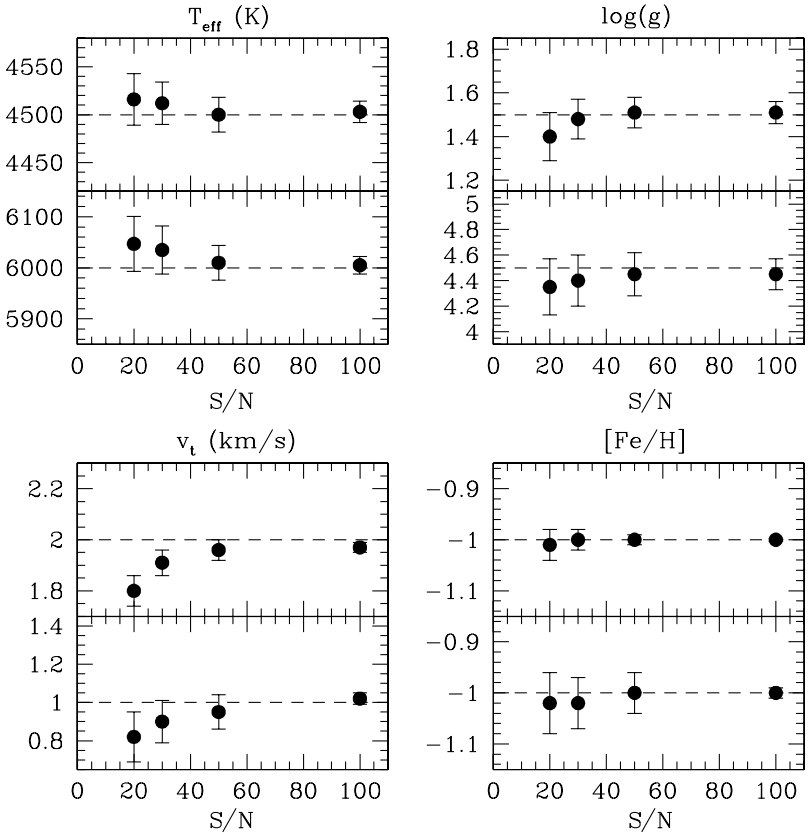

Figure 8. Average values for the recovered atmospheric parameters as a function of S/N for the Monte Carlo samples described in Section 7.1. Upper panels of each window show the results for the giant star model, while lower panels show the results for the dwarf stars. Error bars are the dispersion by the mean. Dashed lines are the original value for each parameter.

To summarize, when the full optimization process is completed, GALA will provide for each analyzed element the (weighted) mean abundance, the dispersion and the number of lines used (which provide the statistical uncertainty), the net variation in abundance due to the new optimization with $T_{\rm eff} + \sigma_{T_{\rm eff}}$ and that with $T_{\rm eff} - \sigma_{T_{\rm eff}}$ (which provides the uncertainty owing to the choice of stellar parameters). Also, for each atmospheric parameter the quoted internal uncertainties are computed. Finally, the quality parameter $F_{\rm merit}$ is provided to evaluate the goodness of the solution as a whole.

7. DEPENDENCE ON S/N

We performed a number of experiments to test the stability and reliability of the derived atmospheric parameters with GALA at different noise conditions. We performed two kind of experiments described below. The first is based on a grid of synthetic spectra of abundances and atmospheric parameters known a priori in order to estimate the reliability of the code as a function of the parameters and the S/N. The second group of tests is based on real spectra previously analyzed in the literature. In the following, the EWs were measured by means of DAOSPEC (Stetson & Pancino 2008) adopting a Gaussian profile for the line fitting.

7.1. Synthetic Spectra at Different Noise Conditions

With GALA we analyzed a grid of synthetic spectra computed to mimic the UVES at VLT high-resolution spectra with the 580 Red Arm setup. The grid of synthetic spectra includes S/Ns of 20, 30, 50, and 100 per pixel for two different sets of atmospheric parameters: $T_{\rm eff} = 4500$ K, $\log g = 1.5$, $v_t = 2$ km s^{-1}, [M/H] = -1.0 dex to simulate a giant star, and $T_{\rm eff} = 6000$ K, $\log g = 4.5$, $v_t = 1$ km s^{-1}, [M/H] = -1.0 dex to simulate a dwarf star. The spectra were computed with the following procedure.

1. For a given model atmosphere, two synthetic spectra were calculated with the SYNTHE code over the wavelength range covered by the two CCDs of the 580 UVES Red Arm grating and then convolved with a Gaussian profile in order to mimic the formal UVES instrumental broadening.
2. The spectra were rebinned to a constant pixel size ($\delta\lambda$ = 0.0147 and 0.0174 pixel Å^{-1} for the lower and upper chips, respectively).
3. The synthetic spectra (normalized to unity) were multiplied with the efficiency curve computed by the FLAMES-UVES ESO Time Calculator in order to model the shape of the templates as realistically as possible.
4. Poissonian noise was injected in the spectra to simulate different noise conditions. Basically, the S/N varies along the spectrum as a function of the efficiency (and thus of the wavelength). The noise was added in any spectrum according to the curve of S/N as a function of λ provided by the FLAMES-UVES ESO Time Calculator. For each S/N a sample of 200 synthetic spectra was generated.

Figure 8 summarizes the average values obtained for each Monte Carlo sample for each atmospheric parameter as a function of S/N; the error bars indicate the dispersion around the mean. Results of the simulations of the giant star model atmosphere are shown in the upper panels of each window, while the lower panels summarize the results for the dwarf star simulations. Basically, the original parameters of the synthetic spectra (marked in Figure 8 as dashed horizontal lines) are

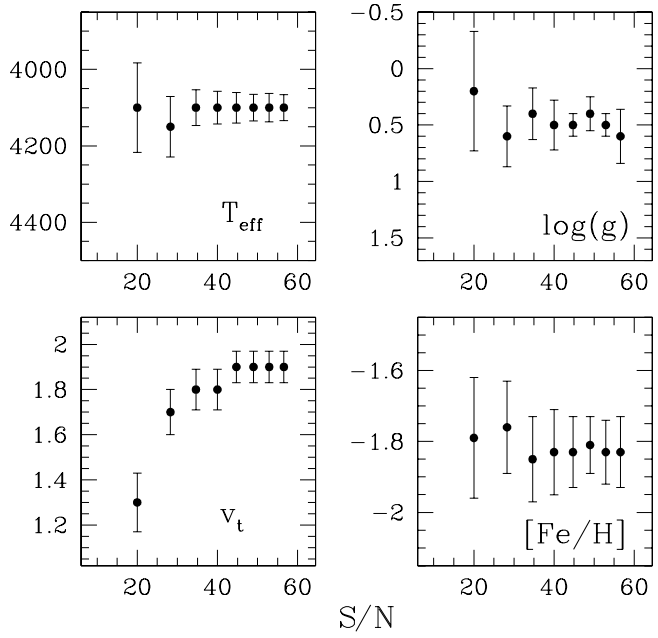

Figure 9. Behavior of the derived atmospheric parameters for the giant star NGC 1786−1501 as a function of S/N obtained by using different UVES co-added spectra. Error bars are derived from the jackknife bootstrapping technique for $T_{\rm eff}$, log g, and v_t, and as dispersion by the mean for [Fe I/H].

recovered with small dispersions and without any significant bias. The major departure from the original values is observed in the microturbulent velocities (both dwarf and giant) at S/N = 20 because of the loss of weak lines.

7.2. Real Echelle Spectra at Different Noise Conditions

The previous test provides an indication about the stability of the method against the S/N, starting with spectra parameters that are known a priori. However, the employed noise model is a simplification because it does not take into account some effects that can also heavily affect the measurement of the EWs, such as the correlation of the noise among adjacent pixels, flat-fielding residuals, failures in the echelle orders merging, and the presence of spectral impurities. Also, the atomic data of the analyzed lines are the same used in the computation of the synthetic spectra, thus excluding from the final line-to-line dispersion random error due to the uncertainty on the atomic data.

In order to provide an additional test of the performance of GALA in conditions with different noise, we performed a simple experiment on the spectra acquired with UVES at FLAMES of the giant star NGC 1786−1501 in the Large Magellanic Cloud (LMC) globular cluster NGC 1786 (see Mucciarelli et al. 2009, 2010). This is a sample of eight spectra with the same exposure time (∼45 minutes) obtained under the same seeing conditions, with a typical S/N per pixel of 20 for each exposure. We used this data set in order to obtain eight spectra with different S/Ns ranging from ∼20 to ∼60 depending on the number of exposures averaged: the spectrum with the lowest S/N is just one exposure and the spectrum with the largest S/N is the average of all eight acquired exposures. The derived parameters for each spectrum are shown in Figure 9 as a function of S/N. The error bars are derived by applying the jackknife bootstrapping technique for $T_{\rm eff}$, log g, and v_t, while for [Fe/H] we used the dispersion by the mean as an estimate of the error.

We note that the parameters are well constrained with small uncertainties for spectra with low S/N: this is not a numerical artifact of the code but it is due to the large number of transitions available in the UVES spectra, coupled with an accurate rejection of the outliers and the use of the uncertainties for each individual line in the slopes' computations. Also, we note that major departures from the final parameters are found again in the determination of v_t at S/N = 20: the derived low value of v_t is due to the fact that at low S/Ns, several weak lines (useful for constraining the microturbulent velocity) are not well measured (then discarded by GALA) or not identified in the noise envelope by DAOSPEC. Note that the derived trend of v_t as a function of S/N shows the same behavior found and discussed by Mucciarelli (2011).

8. AN EFFICIENT APPROACH: ARCTURUS, SUN, HD 84937, AND μLEONIS

In this section we describe a convenient and robust method for performing abundance analysis with GALA, applied to the case of four stars of different metallicity and evolutionary stage and whose parameters are well established among the closest F–G–K stars (namely, the Sun, Arcturus, HD 84937, and μLeonis). We retrieved high-resolution (∼45,000) spectra from the ESO[11] (for the Sun, Arcturus, and HD 84937) and ELODIE[12] (for μLeonis) archives.

8.1. Selection of the Lines

For each star we defined a suitable line list of Fe I and Fe II transitions, starting from the most updated version of the Kurucz/Castelli lines data set.[13] We apply an iterative procedure to define the line list. Assuming that the parameters of the targets are not known a priori, we performed a first analysis by using a preliminary line list including only laboratory transitions with $\chi < 6$ eV and log $(gf) > -5$ dex. Such a line list is not checked against the spectral blendings arising from the adopted spectral resolution and the atmospheric parameters and it is used only to perform a preliminary analysis. With the new parameters derived we define a new line list for each star. The lines are selected by the inspection of synthetic spectra computed with the new parameters and convolved with a Gaussian profile in order to reproduce the observed spectral resolution. At this step, only iron transitions predicted to be unblended are taken into account and used for the new analysis.

8.2. EW Measurements

EWs are measured by using the code DAOSPEC which adopts a saturated Gaussian function to fit the line profile and a unique value for the FWHM for all the lines. We start with the FWHM derived from the nominal spectral resolution of the spectra, leaving DAOSPEC free to readjust the value of FWHM according to the global residual of the fitting procedure. The measurement of EWs is repeated using the optimized FWHM value as a new input value until convergence is reached at a level of 0.1 pixel. The formal error of the fit provided by DAOSPEC is used as 1σ uncertainty on the EW measurement.

[11] http://archive.eso.org/eso/eso_archive_main.html
[12] http://atlas.obs-hp.fr/elodie/
[13] http://wwwuser.oat.ts.astro.it/castelli/linelists.html

Table 1
Iron Abundance (from Neutral and Singly Ionized Lines) and Atmospheric Parameters Derived with GALA for Arcturus, μLeonis, the Sun, and HD 84937

Star	[Fe I/H] (dex)	[Fe II/H] (dex)	$T_{\rm eff}$ (K)	log g	v_t (km s^{-1})
Sun	$-0.01^{+0.02}_{-0.03} \pm 0.009$	$+0.01^{+0.03}_{-0.07} \pm 0.003$	5800 ± 64	4.50 ± 0.18	1.20 ± 0.13
Arcturus	$-0.51^{+0.05}_{-0.04} \pm 0.007$	$-0.52^{+0.03}_{-0.05} \pm 0.015$	4300 ± 60	1.60 ± 0.06	1.50 ± 0.06
HD 84937	$-2.28^{+0.06}_{-0.04} \pm 0.007$	$-2.27^{+0.05}_{-0.04} \pm 0.020$	6150 ± 56	3.20 ± 0.13	0.70 ± 0.24
μLeonis	$+0.37^{+0.04}_{-0.06} \pm 0.011$	$+0.38^{+0.04}_{-0.08} \pm 0.033$	4500 ± 81	2.40 ± 0.26	1.40 ± 0.07
Sun	0.00	0.00	5778	4.438	0.8–1.35
Arcturus	-0.52 ± 0.02	-0.40 ± 0.03	4286 ± 30	1.66 ± 0.05	1.74
HD 84937	-2.14 ± 0.17	...	6251 ± 94	3.97 ± 0.18	0.8–1.7
μLeonis	$+0.28 \pm 0.13$	...	4504 ± 121	2.33 ± 0.27	1.2–2.2

Notes. For the abundances, the first two error bars are the uncertainties arising from the atmospheric parameters following the prescriptions by Cayrel et al. (2004), while the last one is the internal error calculated as $\sigma/\sqrt{(N_{\rm lines})}$. The uncertainties in the derived atmospheric parameters are computed with a jackknife bootstrapping technique. In the lower part of the table, the values available in the literature are listed for comparison.

8.3. Analysis with GALA

The program stars are analyzed by employing all three working blocks, requiring a spectroscopic optimization of $T_{\rm eff}$, log g, v_t, and [M/H] and in all cases starting with the same set of guessed parameters (namely, $T_{\rm eff} = 5000$, log $g = 2.5$, [M/H] $= -1.0$ dex, and $v_t = 1.5$ km s^{-1}). The optimization is performed by exploring the parameter space in small steps of $\delta T_{\rm eff} = 50$ K, δlog $g = 0.1$, and $\delta v_{\rm t} = 0.1$ km s^{-1}; the metallicity is investigated by adopting the step of the ATLAS9 grids (δ[M/H] $= 0.5$ dex).

In the first run, we analyzed the program stars assuming the same configuration for the input parameters of GALA; in particular, we included only lines with $\sigma_{\rm EW} < 10\%$ and with EWR > -5.8 (corresponding to $\sim$10 mÅ at 6000 Å). After a first run of GALA, we refined the maximum EWR allowed which depends mainly on the onset of the saturation along the curve of growth (and thus is different for stars with different atmospheric parameters). We adopted a maximum allowed value of EWR $= -4.65$ for Arcturus and μLeonis and -4.95 for the Sun and HD 84937. These values were chosen on the basis of visual inspection of the curve of growth, in order to exclude too strong lines, for which the Gaussian approximation can fail. After the first run of GALA, the line list is refined by using the new parameters obtained by GALA as described above and the procedure is repeated. Table 1 summarizes the derived atmospheric parameters (with the corresponding jackknife uncertainties) and the [Fe/H] I and [Fe/H] II abundance ratios, together with the two error bars due to the atmospheric parameters and the internal error computed as $\sigma/\sqrt{(N_{\rm lines})}$.

We compare our results with those available in the literature (and listed in Table 1 as references). For the Sun we derive $T_{\rm eff} = 5800 \pm 64$ K, log $g = 4.50 \pm 0.18$, $v_t = 1.20 \pm 0.13$ km s^{-1}, and [Fe/H] $= -0.01 \pm 0.03$ dex (where the error bar is the sum in quadrature of the individual uncertainties listed in Table 1). Our results for $T_{\rm eff}$ and log g agree very well with those listed in the compilation on the NASA Web site.[14] Concerning the microturbulent velocities, values available in the literature range from 0.8 km s^{-1} (Biemont et al. 1981) to 1.35 km s^{-1} (Steffen et al. 2009). A value of 1 km s^{-1} is typically adopted as representative for the Sun in several chemical analyses (see Caffau et al. 2011).

Our analysis of Arcturus provides $T_{\rm eff} = 4300 \pm 60$ K, log $g = 1.60 \pm 0.06$, and $v_t = 1.50 \pm 0.06$ km s^{-1}, with an iron abundance [Fe/H] $= -0.51 \pm 0.05$. These results well match the recent analysis of Arcturus by Ramirez & Allende Prieto (2011) which provides an accurate determination of the atmospheric parameters and the chemical composition; in particular, $T_{\rm eff}$ and log g are derived in an independent way with respect to our approach, finding $T_{\rm eff} = 4286 \pm 30$ K (by fitting the observed spectral energy distribution), log $g = 1.66 \pm 0.05$ (through the trigonometric parallax), while v_t turns out to be 1.74 km s^{-1} (by using the same approach used in GALA). The final iron abundance is [Fe/H] $= -0.52 \pm 0.04$ dex. In both cases, the agreement with the literature values is good. Finally, Figure 10 shows an example of the graphical output of GALA for Arcturus.

For HD 84937 we derive $T_{\rm eff} = 6150 \pm 56$ K, log $g = 3.20 \pm 0.13$, $v_t = 0.70 \pm 0.24$ km s^{-1}, and [Fe/H] $= -2.28 \pm 0.06$ dex, while for μLeonis we obtain $T_{\rm eff} = 4500 \pm 81$ K, log $g = 2.40 \pm 0.26$, $v_t = 1.40 \pm 0.07$ km s^{-1}, and [Fe/H] $= +0.37 \pm 0.06$ dex. For these two stars, several determinations are available in the literature and we decide to use the average of the values listed in the classical compilation by Cayrel de Strobel et al. (2001) as a reference, $T_{\rm eff} = 6251 \pm 94$ K, log $g = 3.97 \pm 0.18$, and [Fe/H] $= -2.14 \pm 0.17$ dex for HD 84937 and $T_{\rm eff} = 4504 \pm 121$ K, log $g = 2.33 \pm 0.27$, and [Fe/H] $= +0.28 \pm 0.13$ dex for μLeonis. Note that the value of the microturbulent velocities is omitted by Cayrel de Strobel et al. (2001) because the authors listed in their compilation use different definitions for this parameter (see Mucciarelli 2011 for a review of the different approaches) or assume a representative value. For HD 84937, the values of v_t range from 0.8 up to 1.7 km s^{-1}, while our value is slightly lower. Also, for μLeonis, the range of values for v_t is wide (from 1.2 up to 2.2 km s^{-1}) but our value agrees with this range. Basically, the agreement with the values listed by Cayrel de Strobel et al. (2001) is good, but for the gravity of HD 84937, for which we derive a lower value, this difference can be partially explained in light of the different values of v_t.

8.4. Stability Against the Initial Parameters

A relevant feature of an automatic procedure to infer parameters and abundances is its stability against the input atmospheric parameters. In order to assess the effect of different first-guess parameters, we analyze the spectrum of Arcturus by investigating a regular grid of input parameters with $T_{\rm eff}$ ranging from 3800 to 4800 K (in steps of 100 K) and log g from 1.0 to 2.2 (in steps of 0.1). Figure 11 shows the grid of the input parameters in the $T_{\rm eff}$–log g plane (empty points) with the position of the derived parameters (black points); the upper panel summarizes

[14] http://nssdc.gsfc.nasa.gov/planetary/factsheet/sunfact.html

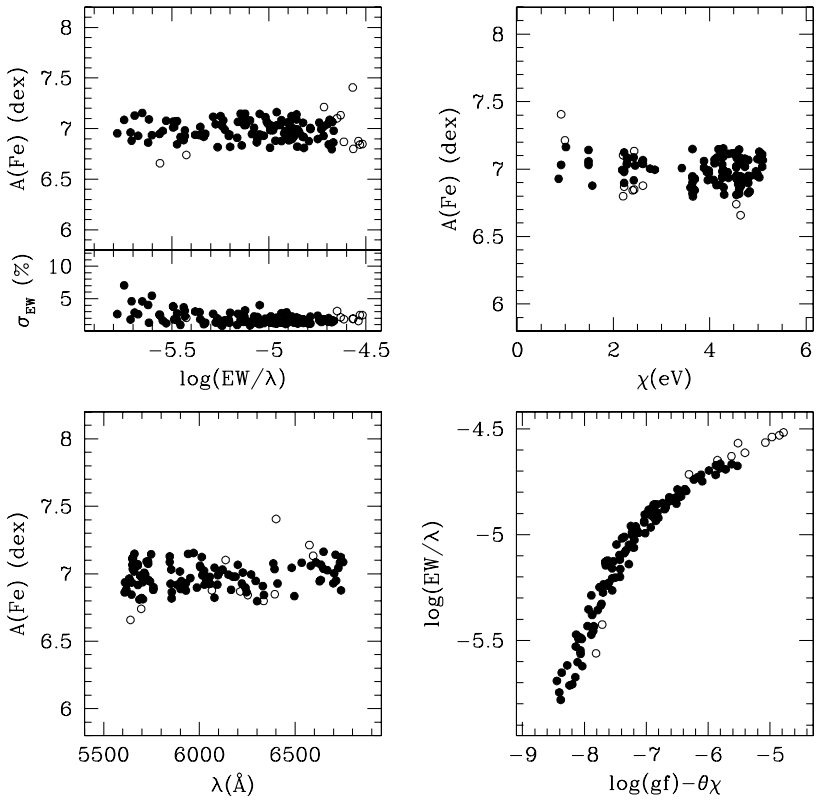

Figure 10. Example of the graphical output of GALA for Arcturus (see Section 8): black circles are the Fe I lines used in the analysis and the empty circles show rejected points.

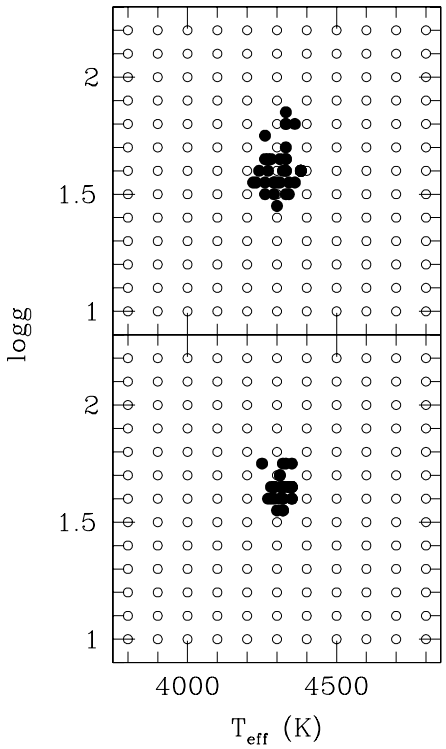

Figure 11. Position of the final parameters for Arcturus (black points) in the $T_{\rm eff}$–log g plane, in comparison with the input parameters (empty circles) obtained by using GALA without (upper panel) and with (lower panel) the refinement working block.

the results when GALA is used without the refinement working block, while the lower panel shows the results obtained by also employing the refinement option. The recovered parameters cover a small range: in the first run the dispersion of the mean is 46 K for $T_{\rm eff}$ and 0.09 for log g, while these values drop to 25 K and 0.05, respectively, when the refinement working block is enabled.

9. A TEST WITH GLOBULAR CLUSTERS

Globular clusters are ideal templates for checking the capability of our procedure to derive reliable atmospherical parameters because of the homogeneity (in terms of metallicity, age, and distance) of their stellar content. Thus, the derived parameters for stars in a given globular cluster can be easily compared with theoretical isochrones in the $T_{\rm eff}$–log g plane.

We apply the same procedure described in Section 8 to analyze a set of high-resolution spectra for stars in the globular cluster NGC 6752, ranging from the turn-off up to the bright portion of the red giant branch. The spectra have been retrieved by the ESO archive[15] and reduced with the standard ESO pipeline.[16] They are from different observing programs and have different S/Ns, including giant stars crossing the red giant branch bump region observed with UVES at the VLT (slit mode) within the ESO Large Program 65.L-0165 with very high (>200) S/N, the stars in the bright portion of the red giant branch observed with UVES-FLAMES at the VLT (fiber mode) within the Galactic globular clusters survey presented by Carretta et al. (2009) and the dwarf/subgiant stars observed with UVES at the VLT (slit mode) within the ESO Large Program 165.L-0263.

The main panel of Figure 12 shows the position of the final parameters derived with GALA in the $T_{\rm eff}$–log g plane. Also, two theoretical isochrones with an age of 12 Gyr and a metallicity

[15] http://archive.eso.org/cms/eso-data.html
[16] http://www.eso.org/sci//software/pipelines/

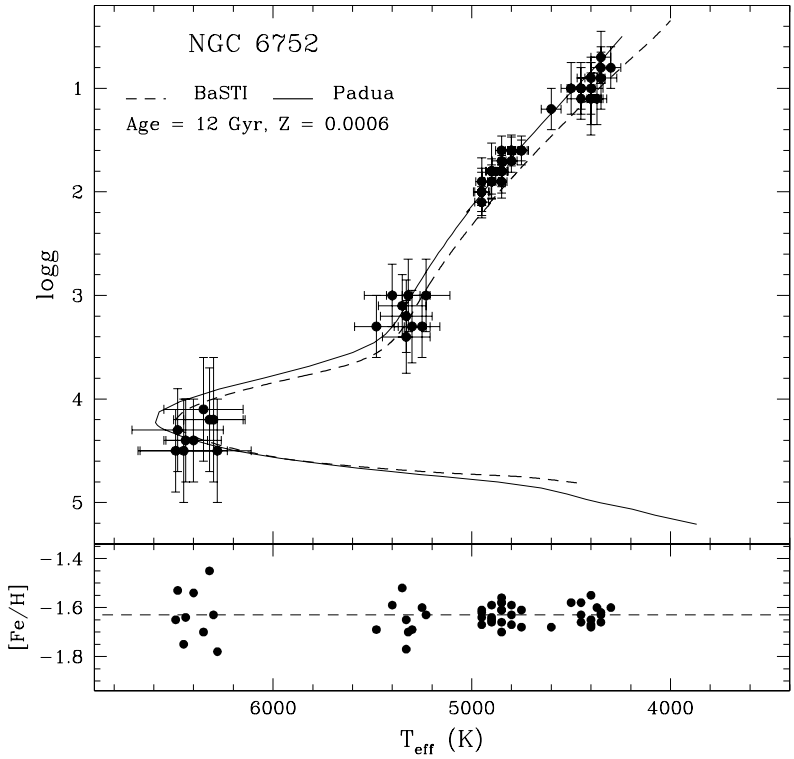

Figure 12. Main panel: position in the $T_{\rm eff}$–log g plane of the stars in the globular cluster NGC 6752 analyzed with GALA. We plotted as references two isochrones computed with an age of 12 Gyr and a metallicity of $Z = 0.0006$ (assuming an α-enhancement chemical mixture), from the BaSTI (Pietrinferni et al. 2006, dotted curve) and Padua (Girardi et al. 2000, solid curve) database. Lower panel: behavior of the [Fe/H] ratio as a function of $T_{\rm eff}$.

of $Z = 0.0006$ (assuming an α-enhanced chemical mixture) are shown as reference (the gray curve is from the BaSTI database by Pietrinferni et al. 2006 and the black curve is from the Padua database by Girardi et al. 2000). In the lower panel, we show the behavior of the [Fe/H] ratio as a function of $T_{\rm eff}$. No significant trend is found while the star-to-star scatter increases with increasing $T_{\rm eff}$ because of the lower S/N.

The parameters derived with GALA well reproduce the behavior predicted by the theoretical models for an old simple stellar population with the same metallicity of the cluster, confirming the physical reliability of the final solution. Also, we note that the error bars, both in $T_{\rm eff}$ and log g, change according to the quality of the spectra, ranging from ∼30 K and ∼0.15 for the giants with the highest S/N up to ∼200 K and ∼0.5 for the dwarf stars with lower S/N.

The entire sample of 52 stars provides an average iron abundance of [Fe/H]I $= -1.63$ dex ($\sigma = 0.06$ dex). This value is consistent with the previous estimates available in the literature which point out an iron content ranging from [Fe/H] $= -1.62$ (Grundahl et al. 2002) up to [Fe/H] $= -1.42$ dex (Gratton et al. 2001). In this comparison we cannot take into account the different adopted solar values.

The stars in common with Carretta et al. (2009) show a reasonable agreement in the atmospheric parameters, with $T_{\rm eff}^{\rm GALA} - T_{\rm eff}^{\rm Carretta} = +49$ K ($\sigma = 42$ K), $\log g^{\rm GALA} - \log g^{\rm Carretta} = -0.26$ ($\sigma = 0.07$), and $[{\rm Fe/H}]^{\rm GALA} - [{\rm Fe/H}]^{\rm Carretta} = -0.08$ dex ($\sigma = 0.05$ dex).

Also, for the stars in common with Yong et al. (2005), the agreement is excellent (also because these spectra have very high S/N and a large wavelength coverage, thus permitting measurements of a large number of Fe I and Fe II lines): $T_{\rm eff}^{\rm GALA} - T_{\rm eff}^{\rm Yong} = -1$ K ($\sigma = 32$ K), $\log g^{\rm GALA} - \log g^{\rm Yong} = -0.39$ ($\sigma = 0.11$), and $[{\rm Fe/H}]^{\rm GALA} - [{\rm Fe/H}]^{\rm Yong} = +0.00$ dex ($\sigma = 0.06$ dex).

The comparison with the analysis of the turn-off and subgiant branch stars by Gratton et al. (2001) is not trivial because they derived the atmospheric parameters from median spectra for the two groups of stars. The temperatures have been derived by fitting the wings of the Hα, while the gravities have been obtained from the positions of the stars in the color–magnitude diagram. When we compared the parameters by Gratton et al. (2001) with the average values obtained by our analysis of individual stars, the agreement was not perfect but consistent within the uncertainties: we found $\langle T_{\rm eff}^{\rm GALA}\rangle - T_{\rm eff}^{\rm Gratton} = +164$ K, $\langle \log g^{\rm GALA}\rangle - \log g^{\rm Gratton} = +0.06$, and $[{\rm Fe/H}]^{\rm GALA} - [{\rm Fe/H}]^{\rm Gratton} = -0.19$ dex ($\sigma = 0.15$ dex) for the turn-off stars, and $\langle T_{\rm eff}^{\rm GALA}\rangle - T_{\rm eff}^{\rm Gratton} = -15$ K, $\langle \log g^{\rm GALA}\rangle - \log g^{\rm Gratton} = -0.36$, and $[{\rm Fe/H}]^{\rm GALA} - [{\rm Fe/H}]^{\rm Gratton} = -0.23$ dex ($\sigma = 0.11$ dex) for the subgiant stars.

10. SUMMARY

In this paper we have presented a new, automatic tool for performing an accurate analysis of stellar spectra. GALA is designed to automatically search for the best atmospheric parameters $T_{\rm eff}$, log g, $v_{\rm t}$, and the overall metallicity [M/H] for moderate- and high-resolution stellar absorption spectra using the EWs of metallic lines. Also, GALA provides the abundance of each individual line for which the user provides the EW, as well as the average abundance for each atomic species.

The source code of GALA is freely available at the Web site http://www.cosmic-lab.eu/Cosmic-Lab/Products.html together with the user manual (including information about installation, configuration of the input files, and how to obtain and properly

use the model atmospheres) and an example of the input files provided as a reference. The main advantages of the code are the following.

1. The capability to optimize all the parameters or only part of them. The code is versatile in order to perform different kinds of analysis (full or partial spectroscopic analysis, experiments about the guessed parameters, etc.) and adopt different recipes for deriving $\log g$.
2. The capability to perform a careful rejection of the outliers according to the line strength, the EW quality, and the line distribution in the A(Fe)–χ and A(Fe)–EWR planes.
3. The capability to estimate for each individual star the internal errors for (a) the optimized parameters by adopting the jackknife bootstrapping technique and (b) the derived uncertainties due to the choice of atmospheric parameters, following both the prescriptions by Cayrel et al. (2004) and the classical method of altering one parameter at a time.

We have performed an extensive set of tests with both synthetic and observed spectra in order to assess the performances of the code.

1. Experiments with synthetic spectra (whose atmospheric parameters are known a priori) with the injection of Poissonian noise to simulate different noise conditions show a high stability of the code in recovering the atmospheric parameters without significant bias. The major departure from the original values is found in the microturbulent velocity of low ($\sim$20) S/N spectra, due to the systematic loss of weak lines.
2. A set of FLAMES-UVES spectra of the LMC giant star NGC 1786−1501 observed with different values of S/N (from $\sim$20 up to $\sim$60) has been analyzed with GALA, confirming that our procedure also well constrains the parameters in the case of low spectral quality. Also in this case, we found that the largest departures are for microturbulent velocity in spectra with low S/N because the weak lines are not well measured or not detectable in the noise envelope, leading to an underestimate of this parameter.
3. We analyzed four stars (namely, the Sun, Arcturus, HD 84937, and μLeonis) of different metallicity and evolutionary stage and whose parameters are well established among the closest F–G–K stars. We described an efficient method (including the line selection, the measurement of the EWs, and the chemical analysis) to best exploit the capabilities of GALA. Our results for these stars (both for atmospheric parameters and [Fe/H] ratio) agree well with those available in the literature.
4. Finally, we analyzed a sample of 52 stars of the Galactic globular cluster NGC 6752 in different evolutionary stages. The derived $T_{\rm eff}$ and $\log g$ follow well the predictions of theoretical isochrones with the appropriate age and chemical composition for this cluster. Also, the derived iron content nicely agrees with the previous estimates from other works.

The code permits us to obtain chemical abundances and atmospheric parameters for large stellar samples in a very short time, thus making GALA a useful tool in the epoch of multi-object spectrographs and large surveys. Because of its open source code nature, changes to GALA will be implemented in the next releases according to feedback from users. In particular, we plan to include new grids of opacity distribution functions and models that will be publicly released in the future. Also, GALA will be constantly updated in order to include variations and changes in ATLAS9 and MARCS models as well as in the ATLAS9 code.

The authors warmly thank Fiorella Castelli, Thomas Masseron, Piercarlo Bonifacio, and Andrea Negri for useful comments, discussions, and suggestions. We thank the anonymous referee for a careful reading of the paper and helpful comments. This research is part of the project COSMIC-LAB funded by the European Research Council (under contract ERC-2010-AdG-267675).

"Und wenn dich das Irdische vergaß, zu der stillen Erde sag: Ich rinne. Zu dem raschen Wasser sprich: Ich bin." (R. M. Rilke 1923, Die Sonette an Orpheus, II, XXIX).

REFERENCES

Allende Prieto, C., Majewski, S. R., Schiavon, R., et al. 2008, AN, 329, 1018
Barden, S. C., Jones, D. J., Barnes, S. I., et al. 2010, Proc. SPIE, 7735, 8
Biemont, E., Grevesse, N., Hannaford, P., & Lowe, R. M. 1981, ApJ, 248, 867
Bonifacio, P., & Caffau, E. 2003, A&A, 399, 1183
Caffau, E., Ludwig, H.-G., Steffen, M., Freytag, B., & Bonifacio, P. 2011, SoPh, 268, 251
Carretta, E., Bragaglia, A., Gratton, R., & Lucatello, S. 2009, A&A, 505, 139
Castelli, F. 1988, Oss. Astron. Trieste, 1164 (http://atmos.obspm.fr/images/stories/download/castelli0607.pdf)
Castelli, F. 2005a, MSAIS, 8, 25
Castelli, F. 2005b, MSAIS, 8, 44
Castelli, F., & Kurucz, R. L. 2004, arXiv:astro-ph/0405087
Cayrel, R., Depagne, E., Spite, M., et al. 2004, A&A, 416, 1117
Cayrel de Strobel, G., Soubiran, C., & Ralite, N. 2001, A&A, 373, 159
Cirasuolo, M., Afonso, J., Bender, R., et al. 2011, Msngr, 145, 11
de Jong, R. 2011, Msngr, 145, 14
Edvardsson, B. 1988, in IAU Symp., 132, The Impact of Very High S/N Spectroscopy on Stellar Physics, ed. G. Cayrel de Strobel & M. Spite (Dordrecht: Kluwer), 387
Fitzpatrick, M. J., & Sneden, C. 1987, BAAS, 19, 1129
Fontenla, J. M., Avrett, E. H., & Loeser, R. 1993, ApJ, 406, 319
Freeman, K., Ness, M., Wylie-de-Boer, E., et al. 2013, MNRAS, 428, 3660
Gilmore, G., Randich, S., Asplund, M., et al. 2012, Msngr, 147, 25
Girardi, L., Bressan, A., Bertelli, G., & Chiosi, C. 2000, A&AS, 141, 371
Gratton, R. G., Bonifacio, P., Bragaglia, A., et al. 2001, A&A, 369, 87
Grundahl, F., Briley, M., Nissen, P. E., & Feltzing, S. 2002, A&A, 385, L14
Gustafsson, B., Edvardsson, B., Eriksson, K., et al. 2008, A&A, 486, 951
Kunder, A., Koch, A., Rich, R. M., et al. 2012, AJ, 143, 57
Kurucz, R. L. 2005, MSAIS, 8, 14
Lupton, R. 1993, in Statistics in Theory and Practice (Princeton, NJ: Princeton Univ. Press)
Masseron, T. 2006, PhD thesis, Observatoire de Paris
Mészáros, Sz., Allende Prieto, C., Edvardsson, B., et al. 2012, AJ, 144, 120
Mucciarelli, A. 2011, A&A, 528, 44
Mucciarelli, A., Origlia, L., & Ferraro, F. R. 2010, ApJ, 717, 277
Mucciarelli, A., Origlia, L., Ferraro, F. R., & Pancino, E. 2009, ApJL, 695, L134
Pietrinferni, A., Cassisi, S., Salaris, M., & Castelli, F. 2006, ApJ, 642, 797
Posbic, H., Katz, D., Caffau, E., et al. 2012, A&A, 544, A154
Press, W. H., Teukolsky, A. A., Vetterling, W. T., & Flannery, B. P. 1992, Numerical Recipes (2nd ed.; Cambridge: Cambridge Univ. Press)
Ramirez, I., & Allende Prieto, C. 2011, ApJ, 743, 135
Ramirez, S. V., Cohen, J. G., Buss, J., & Briley, M. M. 2001, AJ, 122, 1429
Recio-Blanco, A., Bijaoui, A., & de Laverny, P. 2006, MNRAS, 370, 141
Sbordone, L., Bonifacio, P., Caffau, E., & Ludwig, H. G. 2010, in Proc. 11th Symp. Nuclei in the Cosmos, in press (arXiv:1009.5210)
Sbordone, L., Bonifacio, P., Castelli, F., & Kurucz, R. L. 2004, MSAIS, 5, 93
Sousa, S. G., Santos, N. C., Israelian, G., Mayor, M., & Monteiro, M. J. P. F. G. 2007, A&A, 469, 783
Steffen, M., Ludwig, H.-G., & Caffau, E. 2009, MSAIS, 80, 731
Steinmetz, M., Zwitter, T., Siebert, A., et al. 2006, AJ, 132, 1645
Stetson, P. B., & Pancino, E. 2008, PASP, 120, 1332
Valenti, J. A., & Piskunov, N. 1996, A&AS, 118, 595
Yong, D., Grundahl, F., Nissen, P. E., Jensen, H. R., & Lambert, D. L. 2005, A&A, 438, 875